On the spectrum of soil moisture from hourly to interannual scales

Gabriel G. Katul,[1,2] Amilcare Porporato,[1,2] Edoardo Daly,[1,2] A. Christopher Oishi,[1] Hyun-Seok Kim,[1] Paul C. Stoy,[1] Jehn-Yih Juang,[1] and Mario B. Siqueira[1,3]

Received 17 July 2006; revised 8 January 2007; accepted 25 January 2007; published 22 May 2007.

[1] The spectrum of soil moisture content at scales ranging from 1 hour to 8 years is analyzed for a site whose hydrologic balance is primarily governed by precipitation (p), and evapotranspiration (ET). The site is a uniformly planted loblolly pine stand situated in the southeastern United States and is characterized by a shallow rooting depth (R_L) and a near-impervious clay pan just below R_L. In this setup, when ET linearly increases with increasing root zone soil moisture content (θ), an analytical model can be derived for the soil moisture content energy spectrum ($E_s(f)$, where f is frequency) that predicts the soil moisture "memory" (taken as the integral timescale) as $\beta_1^{-1} \approx \eta R_L/\mathrm{ET}_{\max}$, where $\mathrm{ET}_{\max}$ is the maximum measured hourly ET and η is the soil porosity. The spectral model suggests that $E_s(f)$ decays at $f^{-2-\alpha}$ at high f but almost white (i.e., f^0) at low f, where α is the power law exponent of the rainfall spectrum at high f ($\alpha \approx 0.75$ for this site). The rapid $E_s(f)$ decay at high f makes the soil moisture variance highly imbalanced in the Fourier domain, thereby permitting much of the soil moisture variability to be described by a limited number of Fourier modes. For the 8-year data collected here, 99.6% of the soil moisture variance could be described by less than 0.4% of its Fourier modes. A practical outcome of this energy imbalance in the frequency domain is that the diurnal cycle in ET can be ignored if β_1^{-1} (estimated at 7.6 days from the model) is much larger than 12 hours. The model, however, underestimates the measured $E_s(f)$ at very low frequencies ($f \ll \beta_1$) and its memory, estimated from the data at 42 days. This underestimation is due to seasonality in $\mathrm{ET}_{\max}$ and to a partial decoupling between ET and soil moisture at low frequencies.

Citation: Katul, G. G., A. Porporato, E. Daly, A. C. Oishi, H.-S. Kim, P. C. Stoy, J.-Y. Juang, and M. B. Siqueira (2007), On the spectrum of soil moisture from hourly to interannual scales, *Water Resour. Res.*, *43*, W05428, doi:10.1029/2006WR005356.

1. Introduction

[2] Over the past two decades, the temporal spectrum of soil moisture (θ) has received significant attention in the climate, hydrologic, and land surface communities because of its impact on a number of processes including terrestrial rainfall [*Delworth and Manabe*, 1988, 1993; *Parlange et al.*, 1992; *Entekhabi et al.*, 1996; *Findell and Eltahir*, 1997; *Koster and Suarez*, 2001; *Wilson et al.*, 2001; *Wu et al.*, 2002, *Chen and Kumar*, 2002; *Lauzon et al.*, 2004; *Koster et al.*, 2004; *Wu and Dickinson*, 2004; *Amenu et al.*, 2005], biogeochemical cycling, and ecosystem resilience [*D'Odorico et al.*, 2003; *Porporato et al.*, 2004]. Because of storage effects within the soil pores, the dynamics of θ posses a memory that is often considerably longer than the integral timescale of many atmospheric processes. Hence climate anomalies can be "sustained" through land surface feedbacks primarily because they can "feed off" on this long-term memory.

[3] The dynamics of θ at a given location depends on the hydrologic balance and on the interplay between variability in incident precipitation (p_i), interception, total evapotransporation (ET), drainage below the root zone, and lateral flow. More indirectly, soil hydraulic properties, hydraulic lift from below the main rooting system, surface heating, and other boundary conditions, such as groundwater table fluctuations or feedback from soil organic matter dynamics (e.g., litter fall, microbial biomass, decomposition), can also shape the spectrum of θ. Studying the joint effects of all these processes on the spectrum of θ remains beyond the scope of a single study. However, a logical starting point is to restrict the θ spectral analysis to two elementary variables shared by all climatic and hydrologic applications: a precipitation forcing (e.g., p_i) and a water loss (e.g., ET). Even within this restrictive scope, analytical theories to predict the spectrum of θ at timescales ranging from hour to interannual have not been fully addressed (mainly due to the lack of data) and frame the objective of this study.

[4] This objective is addressed via a case study using long-term spatially averaged θ collected in a uniform shallow-rooted loblolly pine (*Pinus taeda* L.) plantation (PP) in the southeastern United States. This ecosystem lends itself to a number of simplifying hydrologic assumptions that permit us to explore analytically how variability in p_i and ET shapes the spectrum of θ. A unique data set of half-hourly p_i, ET, and θ measured within the rooting zone

[1]Nicholas School of the Environment and Earth Sciences, Duke University, Durham, North Carolina, USA.
[2]Department of Civil and Environmental Engineering, Pratt School of Engineering, Duke University, Durham, North Carolina, USA.
[3]Departamento de Engenharia Mecânica, Universidade de Brasília, Brasilia, Brazil.

0043-1397/07/2006WR005356$09.00

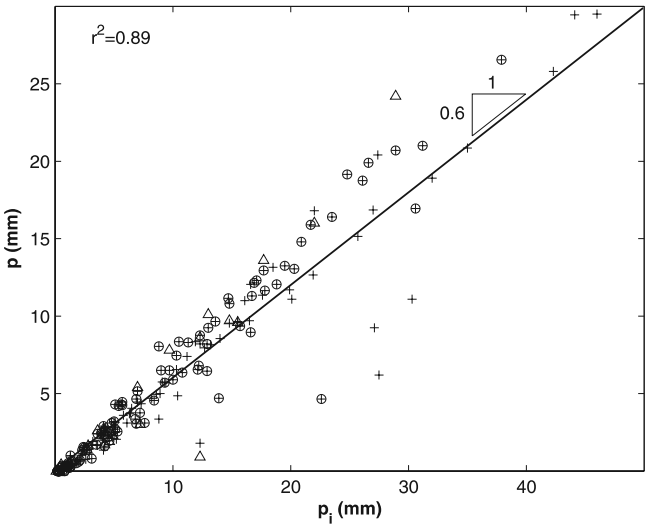

Figure 1. Relationship between daily incident rainfall and throughfall during the years 2004–2005 (r^2 = 0.89). The circles refer to summertime data, and pluses refer to wintertime data. Triangles correspond to measurements starting from May 2005. The seasonal differences in LAI during the year at PP do not play a key role in determining interception.

depth (R_L) has been collected since 1998. This record permits both theoretical and experimental analysis of the interplay between ET and p_i and their concomitant impacts on the spectrum of θ at timescales ranging from hours to years.

2. Experiment

[5] PP is a 24-year old loblolly pine plantation situated in the Blackwood Division of the Duke Forest near Durham, NC (35° 58′ 41.430″N, 79° 05′ 39.087″W, 163 m asl). Long-term mean annual temperature and precipitation at the site are 15.5°C and 1100 mm, respectively. The forest stand lies on Enon silt loam, a low-fertility Hapludalf typical of the southeastern U.S. Piedmont region. An impervious clay pan underlies the research site at ~30 cm belowground [*Oren et al.*, 1998]. PP was established in 1983 following a clear cut and a burn. *P. taeda* seedlings were planted at 2.4 m by 2.4 m spacing and ecosystem development has not been managed after planting. The mean canopy height increased from 14 m in 1998 to 19 m in 2005. The canopy is composed primarily of *P. taeda* with some emergent *Liquidambar styraciflua* L. and a diverse and growing understory with 26 different woody species having diameter at breast height exceeding 2.5 cm.

[6] ET was measured at 20.2 m using an eddy covariance (EC) system composed of a triaxial sonic anemometer (CSAT3, Campbell Scientific, Logan, Utah) and an open path infrared gas analyzer (IRGA, LI-7500, Li-Cor, Lincoln, NE). The 10 Hz measurements of vertical velocity and H_2O concentration were collected and vertical turbulent fluxes were then computed every 30 min. The Webb-Pearman-Leuning (WPL) correction [*Webb et al.*, 1980] for the effects of air density fluctuations on flux measurements was applied to scalar fluxes measured with the open path LI-7500. A closed path gas analyzer (LI-6262, Li-Cor, Lincoln, NE) was employed at PP before 1 May 2001, and 5 Hz measurements were postprocessed as described elsewhere [*Katul et al.*, 1997]. Ancillary meteorological and radiation measurements were also collected and described elsewhere [*Stoy et al.*, 2005]. Topographic variations around the tower are minor (<5%) and negligibly influence the eddy covariance ET flux measurements [*Kaimal and Finnigan*, 1994].

[7] Daily p_i was measured with a rain gauge near the NOAA meteorological station located at a grass clearing adjacent to the PP site. Half-hourly p_i was measured using a tipping bucket (TI, Texas Instruments, Austin, TX) and matched to daily rain gauge data. In the instance of power failures, missing half hourly p_i was gap-filled using daily precipitation from the NOAA station and hourly data from the Chapel Hill airport station.

[8] Integrated 0–30 cm θ measurements were made at 24 locations within the forest stand using CS615 soil moisture sensors (Campbell Scientific, Logan, UT), and then the spatially averaged mean of these measurements was taken to be the site-wide θ every 30 minutes. Interception, as a fraction of incident precipitation, was determined from separate experiments [*Oren et al.*, 1998] and was estimated about 30% of above-canopy rainfall for the years 1998–2000 [*Schäfer et al.*, 2002]. Extensive half-hourly throughfall (p) measurements were also made during the years 2004–2005 with a network of tipping bucket rain gauges (Campbell Scientific) at two different locations and, starting from May 2005, at eight different locations. As shown in Figure 1, using spatially averaged daily rainfall values calculated from these data a linear relationship (regression slope 0.6, r^2 = 0.89) between p_i and p was found, with a resulting interception of about 40% of above-canopy rainfall. The difference between the two estimates of interception (i.e., 30 and 40%) is likely due to the different techniques adopted to measure throughfall. Figure 1 also shows how, at this stand scale, the interception is fairly independent of seasonal variations in leaf area index.

[9] Here we focus on $p_i(t)$, ET(t), and $\theta(t)$ measurements collected from 1998 to 2005 (n = 140,160 data per variable). Key hydroclimatic features during the experimental period included wetter than average growing seasons during 1999, 2000, and 2003, interspersed with an increasingly severe drought, that extended from the summer 2001 until summer 2002, and mild drought conditions in 1998 and 2005. The 2004 April–September growing season precipitation was near the long-term (111 year) mean of 632 ± 130 mm [*Stoy et al.*, 2006]. The measured mean annual p_i and EC-based ET estimates are 1286 mm and 751 mm for the measurement period duration (1998–2005); hence annual ET roughly accounts for about 97% of annual throughfall (771 mm), assuming throughfall is about 60% of incident rainfall. Hence drainage is not a significant contributor to the annual hydrologic balance at this site when compared to rainfall or ET.

3. Theory

3.1. Soil Moisture Dynamics in the Time Domain

[10] The vertically integrated continuity equation for soil moisture across R_L for planar-homogeneous conditions results in

$$\frac{dw(t)}{dt} = p(t) - \mathrm{ET}(t) - D_r(t), \tag{1}$$

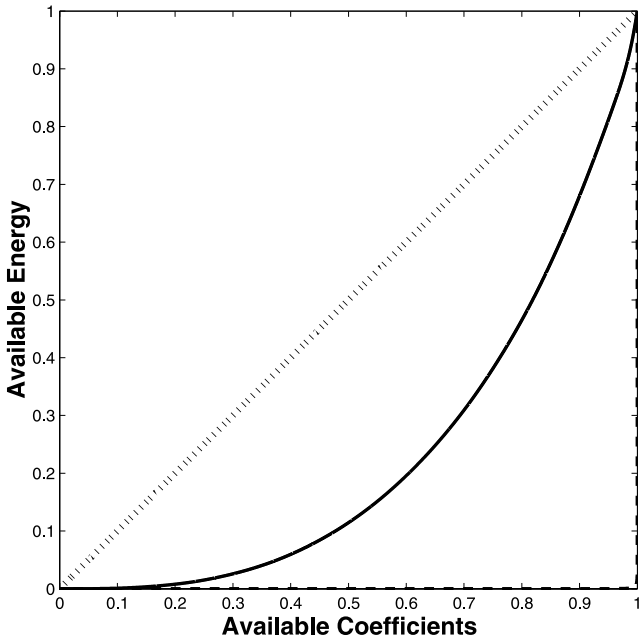

Figure 2. Lorentz curves for the measured soil moisture content time series at PP in the time (solid curve) and Fourier domain (dashed line). The Lorentz curve for a perfectly balanced signal is shown as a 1:1 line (dotted). Note the energy imbalance in the Fourier domain. The point at which a unit loss in a coefficient results in a unit loss in energy for the Lorentz curve in the Fourier domain is at 99.6% of the available coefficients.

where t (in h) is time, $w(t)$ is stored water (in mm), $p(t)$ is, as before, throughfall precipitation (in mm h^{-1}), ET is evapotranspiration (in mm h^{-1}), and D_r is the drainage loss (in mm h^{-1}) below R_L. Defining a total loss function $L(t) = \mathrm{ET}(t) + D_r(t)$, equation (1) can be written as

$$\frac{ds(t)}{dt} + \frac{L(t)}{\eta R_L} = \frac{p(t)}{\eta R_L}, \tag{2}$$

where $s(t) = \theta/\eta = w/(\eta R_L)$ is the degree of saturation ($\in[0, 1]$) and η is soil porosity. If $L(t)$ is assumed to vary only with $s(t)$ [e.g., *Porporato et al.*, 2004], equation (2) can be expressed as

$$\frac{ds(t)}{dt} + \beta_1(s)\, s = \frac{p(t)}{\eta R_L}, \tag{3}$$

with $\beta_1(s) = \dfrac{L_{\max}}{\eta R_L} f(s)$ (in h^{-1}), where L_{max} is the maximum loss rate and $f(s)$ can be interpreted as a dimensionless "shape function" that retains all the higher-order nonlinearities in $L(t)$.

3.2. Soil Moisture Dynamics in the Frequency Domain

[11] Analyzing the soil moisture dynamics in the frequency domain has a number of underexploited advantages over its time domain counterpart. Such advantages are mostly related to the fact that the soil moisture time series appears more "energetically imbalanced" in the frequency domain than in the time domain. In other words, this means that the variability (also referred to as activity or energy) in soil moisture content is "concentrated" in few energetic frequencies (in the Fourier domain) or time instances (in the time domain). To illustrate this point quantitatively using the 8-year measured soil moisture record, the so-called Lorentz curve in both time and frequency domains [*Katul and Vidakovic*, 1996, 1998; *Katul et al.*, 1998] is computed and shown in Figure 2. The Lorentz curve gives a measure of energy imbalance in a given series by using coefficients characterizing the series either in time or frequency domain. In the time domain, these coefficients are simply $s'(t)^2$ for all time instances (where primed quantities indicate departure from the time average). In the frequency domain, they are the amplitudes of the coefficients of the Fourier transform of $s(t)$. The Lorentz curve can be constructed by starting with a ranking of the coefficients from the most to the least energetic and by normalizing them to have energy to be unity (i.e., 100% of the variance is explained by 100% of the coefficients). The curve was generated by sequentially removing the most energetic coefficient and recomputing the energy until all coefficients were removed (thereby making the remaining energy = 0). If all the coefficients in the series contribute equally to the soil moisture variance, the Lorentz curve is the 1:1 line (see Figure 2). If the series is "perfectly unbalanced" (i.e., one coefficient contains or explains all the soil moisture variance), then the Lorentz curve will be composed of two lines: a vertical line bounded by the points (1, 0) and (1, 1) and a horizontal line bounded by (0, 0) and (1, 0).

[12] The Lorentz curves shown in Figure 2 suggest that s in the time domain is closer to a perfectly balanced signal, while in the frequency domain resembles a perfectly unbalanced series. That is, Figure 2 unambiguously shows that the soil moisture dynamics in the Fourier domain require by far less coefficients to explain a specified variance level when compared to their time domain counterpart. As further evidence, we "reconstructed" the soil moisture time series using only the most energetic 0.38% Fourier coefficients and setting the remaining 99.62% to zero. The comparison between the reconstructed and original soil moisture content time series is shown in Figure 3. The good agreement between this reconstructed (n_c = 533 Fourier coefficients) and the originally sampled (n = 140,160 observations) soil moisture series is rather encouraging (regression slope = 0.97, intercept = 0.024, coefficient of determination r^2 = 0.96); the energy loss (defined as the difference in soil moisture variance between the original and reconstructed series) is <0.5%.

[13] The results in Figures 2 and 3 are experimental evidence that variability in root zone soil moisture content in the frequency domain, at scales ranging from 1 hour to multiple years, remains highly imbalanced when compared to its time domain counterpart. Other researchers [e.g., *Wu et al.*, 2002; *Wu and Dickinson*, 2004] found that variability in the deeper layer soil moisture content (from daily to interannual) can also be explained by few Fourier modes. As a consequence, it appears logical to consider equation (3) in the Fourier domain along with its concomitant energy spectrum.

[14] To transform equation (3) from the temporal domain, t, to the frequency domain, f, recall that the Fourier transform of an arbitrary function $h(t)$ is given by

$$H(f) = \int_{-\infty}^{+\infty} h(t)\, e^{ift}\, dt \quad .$$

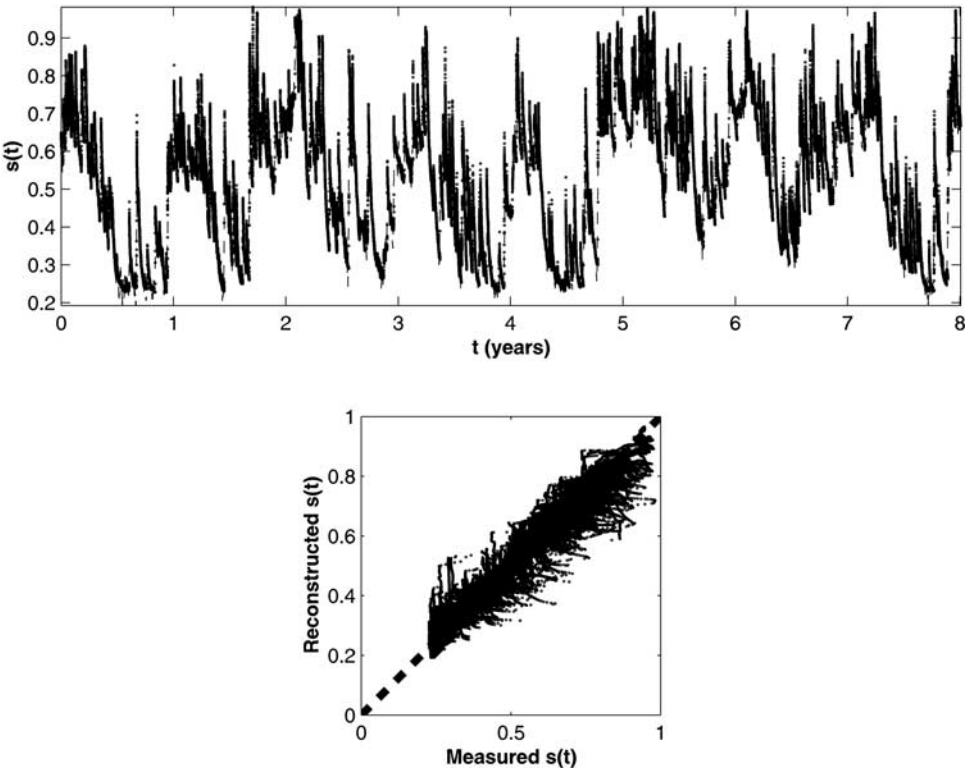

Figure 3. (top) Measured (solid line) degree of saturation (n = 140,146) time series $s(t)$ and the reconstructed series (dashed line) obtained from 0.38% of the Fourier coefficients (n = 533), showing that the two series are almost indistinguishable. (bottom) The 1:1 comparison between the two series is presented for clarity.

By multiplying equation (3) to $e^{i\,f\,t}$ and integrating with respect to time (see *Priestley* [1981] for applicability of such definitions to stationary series), we obtain

$$-if\,S(f) + \int_{-\infty}^{+\infty} \beta_1(s)\,s\,e^{if\,t}dt = P(f), \tag{4}$$

where $S(f)$ and $P(f)$ are the Fourier transforms of $s(t)$ and $p(t)/(\eta R_L)$, respectively.

[15] Since, as shown in Figure 3, the occurrence of $s \approx 1$ is not frequent, surface runoff is neglected. Accordingly, drainage D_r is small when compared to ET, which is assumed to decline linearly from a maximum potential rate $\mathrm{ET_{max}}$ with decreasing s, so that $\mathrm{L_{max}} = \mathrm{ET_{max}}, f(s) = 1$, and $\beta_1 = \dfrac{\mathrm{ET_{max}}}{\eta R_L}$. With such assumptions, which we refer to as the "linear dynamics" case in the following, equation (4) reduces to

$$-if\,S(f) + \beta_1\,S(f) = P(f), \tag{5}$$

resulting in

$$S(f) = \frac{(\beta_1 + if)}{\beta_1^{\,2} + f^2} P(f). \tag{6a}$$

[16] To explore how phase shifts and spectra of soil moisture relate to rainfall, define $r_1(f) = \sqrt{\beta_1^2 + f^2}$ and $\omega_1(f) = \tan^{-1}(f/\beta_1)$, and represent the quantity $\beta_1 + i\,f = r_1(f)e^{i\omega_1}(f)$. Also, when expressing the throughfall spectrum in polar coordinates (i.e., $P(f) = r_2(f)\mathrm{e}^{i\omega_2}(f)$), equation (6a) becomes

$$S(f) = \frac{r_1(f)\,r_2(f)}{\beta_1^{\,2} + f^2}\,\mathrm{e}^{i(\omega_1(f)+\omega_2(f))}. \tag{6b}$$

[17] The term $\mathrm{e}^{i(\omega_1(f)+\omega_2(f))}$ in equation (6b) has important implications in how rainfall variability propagates into the soil moisture system. This term suggests that rainfall and soil moisture variability experience a phase shift given by $\omega_1(f) = \tan^{-1}(f/\beta_1) = \tan^{-1}(f\,R_L\eta/\mathrm{ET_{max}})$. By increasing the rooting zone depth R_L (assuming constant soil porosity and maximum evapotranspiration), the rainfall and soil moisture variability become increasingly out of phase. Furthermore, for long timescales (e.g., decadal), $f \to 0$ and the soil moisture and rainfall variability become approximately in phase with each other. Both findings are qualitatively consistent with the linear phase shift analysis with depth reported by *Amenu et al.* [2005] using the Illinois Climate Network stations.

[18] From equation (6b), the spectrum of s, $E_s(f) = |S(f)|^2$, can be predicted from the spectrum of p, $E_p(f) = |P(f)|^2 = (r_2(f))^2$, using

$$E_s(f) = \frac{(r_1(f))^2(r_2(f))^2}{\left(\beta_1^{\,2} + f^2\right)^2} = \frac{1}{\beta_1^{\,2} + f^2}|P(f)|^2, \tag{7}$$

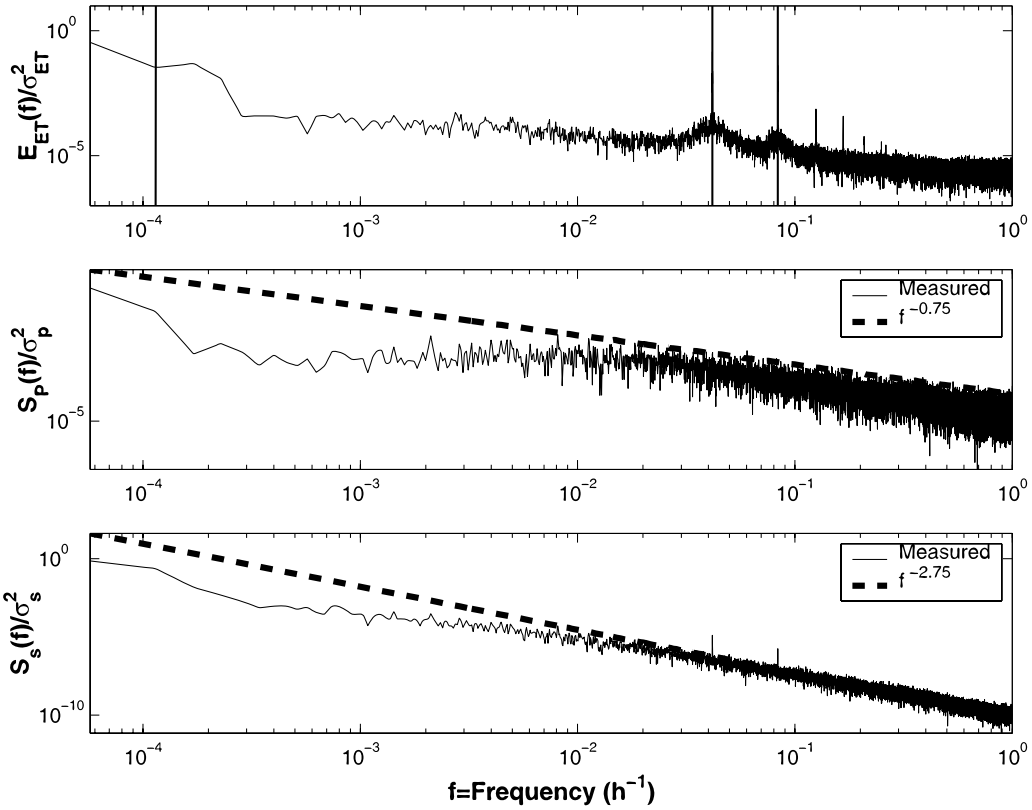

Figure 4. (top) Measured spectra of the eddy covariance ET, (middle) throughfall estimated as a constant fraction of incident precipitation, and (bottom) soil moisture (s) as a function of frequency (f). All spectra are normalized by the variance (σ^2) of their respective time series. The solid vertical lines (right to left) in Figure 4 (top) indicate frequencies corresponding to the following timescales: diurnal (12 hours), daily (24 hours), and annual (8760 hours), respectively. The dashed lines in Figures 4 (middle) and 4 (bottom) indicate the measured exponent α for rainfall (= −0.75) and the predicted exponent (= −2.75) for the soil moisture series at high frequencies.

where $\int_0^\infty E_s(f)\,df = \frac{1}{2}\overline{s'^2}, s' = s - \overline{s}$, and the overbar is time averaging.

[19] Note that if the throughfall time series follows a white noise spectrum, then equation (7) clearly shows how finite storage within the root zone acts as an integrator of short-timescale precipitation anomalies (i.e., large f) transferring their white noise attributes into red noise soil moisture (i.e., $E_s(f) \sim f^{-2}$). However, more revealing is when $E_p(f) = |P(f)|^2 \sim f^{-\alpha}$, as is often the case for storm durations on the order of hours or less. In such a case, $E_s(f)$ behaves as $f^{-2-\alpha}$, decaying much more rapidly than the precipitation spectrum. The $f^{-2-\alpha}$ decay at high frequency might be one plausible reason why the energy in the soil moisture is highly unbalanced in the Fourier domain.

[20] In the following, we compare the measured $E_s(f)$ (shown in Figure 4) with predictions from equation (7) in the linear dynamics case forced by two different forms of rainfall spectrum. In particular, we compare results from the theoretical case of white noise precipitation, in which $E_p(f) = |P(f)|^2 = \phi_p^2$, where ϕ_p is a constant independent of $f(\alpha = 0)$, to the results obtained using the spectrum of precipitation estimated from the data. In the first case, hereafter we refer to as model 1, the spectrum of soil moisture is a constant independent of f when $f \ll \beta_1$ and decays as f^{-2} when $f \gg \beta_1$. In the second case (hereafter referred to as model 2), $E_p(f) = |P(f)|^2$ is estimated using a discrete Fourier transform of the rain gauge time series collected above the canopy multiplied by 0.6 to account for interception losses.

[21] By comparing these two models with measured $E_s(f)$, we can assess how variability in precipitation and nonlinearities in the loss function (i.e., $f(s) \neq 1$) or other low-frequency modulations contribute to the spectrum of soil moisture. In particular, comparing $E_s(f)$ predicted from models 1 and 2 permits us to quantify how the spectrum of $p(t)$ impacts $E_s(f)$ when the loss function maintains its linearity, and comparing model 2 with the measured soil moisture spectrum permits us to assess how nonlinearities in the loss function and other low-frequency sources of variability (e.g., related to pulsed drainage or to seasonality in ET) impact $E_s(f)$.

4. Results and Discussion

[22] Throughout, we refer to the "measured" spectrum of any arbitrary discrete variable X as that spectrum calculated from the raw time series using the Welch's averaged modified periodogram method. In this method, X is divided into overlapping sections, then windowed (Hanning win-

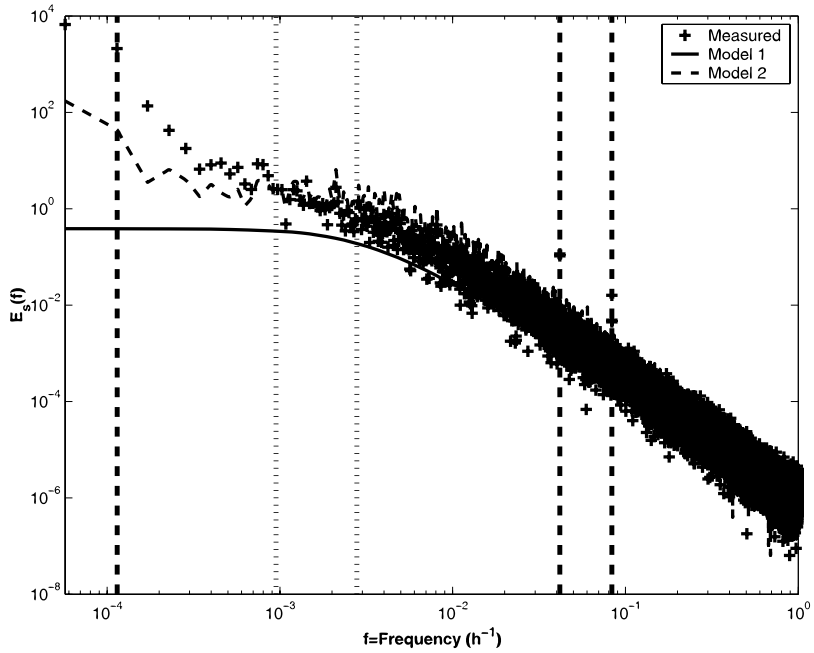

Figure 5. Comparison between measured (pluses) and modeled (lines) soil moisture spectra $E_s(f)$. Model 1 is the linear dynamics model forced with white noise precipitation. Model 2 is the linear dynamics model forced with the measured p spectrum shown in Figure 4. The vertical dotted lines are frequencies corresponding to the following timescales (right to left): β_1^{-1} (= 7.6 days) and the measured integral timescale (= 42 days). The dashed vertical lines (right to left) indicate frequencies corresponding to the following timescales: diurnal (= 12 hours), daily (= 24 hours), and annual (= 8760 hours), respectively.

dows are used), and then zero-padded (when necessary) to permit FFT calculations.

4.1. Spectra of the Hydrologic Variables

[23] Figure 4 shows the normalized spectra of all the key variables for the simplified hydrologic budget, identifying the key timescales and showing the spectral predictions for the exponents at high frequencies. From Figure 4, $E_p(f)$ appears almost "white" at monthly to seasonal timescales, but appears colored at higher frequencies with an exponent approximately equal to -0.75. The measured $E_s(f) \sim f^{-2-0.75}$ seems to confirm power law predictions of model 2 at higher frequencies. The spectrum of ET exhibits the expected peaks at diurnal ($\sim$12 hours) and daily ($\sim$24 hours) frequencies, but significant seasonal and interannual variations are also evident.

4.2. Comparisons Between Measured and Modeled Soil Moisture Spectra

[24] Figure 5 compares the spectrum of measured $E_s(f)$ with predictions by the two models, assuming $\beta_1 = \frac{1}{\eta R_L}\mathrm{ET}_{\max}$, with $\mathrm{ET}_{\max}$ = 0.9 mm h^{-1} directly taken from the EC data (1998–2005), $\eta = 0.55$ and $R_L = 300$ mm taken from *Oren et al.* [1998]. For model 1, we assumed that $E_p(f) = |P(f)|^2 = \phi^2$, where the constant is determined from the measured precipitation variance distributed uniformly at all frequencies (i.e., white noise precipitation spectrum). For model 2, the 30-min measured $E_p(f) = |P(f)|^2$ was used in equation (7). From the comparisons in Figure 5, we note the following:

[25] 1. Model 1 explains several "geometric" attributes of the measured soil moisture spectrum: a near constant value at low frequencies and a rapid decay at high frequencies. However, it is clear that the decay in the measured $E_s(f)$ is steeper than f^{-2} and that model 1 severely underestimates the energy content at frequencies smaller than seasonal (i.e., $f < 0.00035$ h^{-1}).

[26] 2. Model 2 explains all the key geometric attributes of the measured soil moisture spectrum from hours to seasonal reasonably well (see Figure 6 for a 1:1 comparison and statistical analysis; note that the regression slope = 0.93, $r^2 = 0.74$ in a log scale), though it also underestimates the soil moisture variability at frequencies smaller than seasonal. As discussed in Figure 4, the "steepening" of the measured $E_s(f)$ beyond f^{-2} (i.e., $f^{-2.75}$) is well reproduced and is primarily due to the fact that $E_p(f)$ exhibits approximate power law decay of about $f^{-0.75}$ at high frequencies.

[27] For model 1, the correlation time can be estimated analytically as $1/\beta_1$, corresponding to a frequency of $f = 0.0055\ h^{-1}$ (or 7.6 days). This prediction overestimates the frequency (or underestimates the memory) determined from the soil moisture integral timescale, which corresponds to $f \approx 0.001\ h^{-1}$ (or about 42 days) shown in Figure 7. The measured memory or integral timescale was estimated from the area under the measured autocorrelation function of the soil moisture content time series (see Appendix A for derivation). Recall that for model 1, the soil moisture memory is related to the spectral peak in Figure 7 when plotting $fE_s(f)$ versus f (see Appendix A for relationships between β_1, integral timescale, and the frequency at which $fE_s(f)$ peaks). Notwithstanding this underestimation

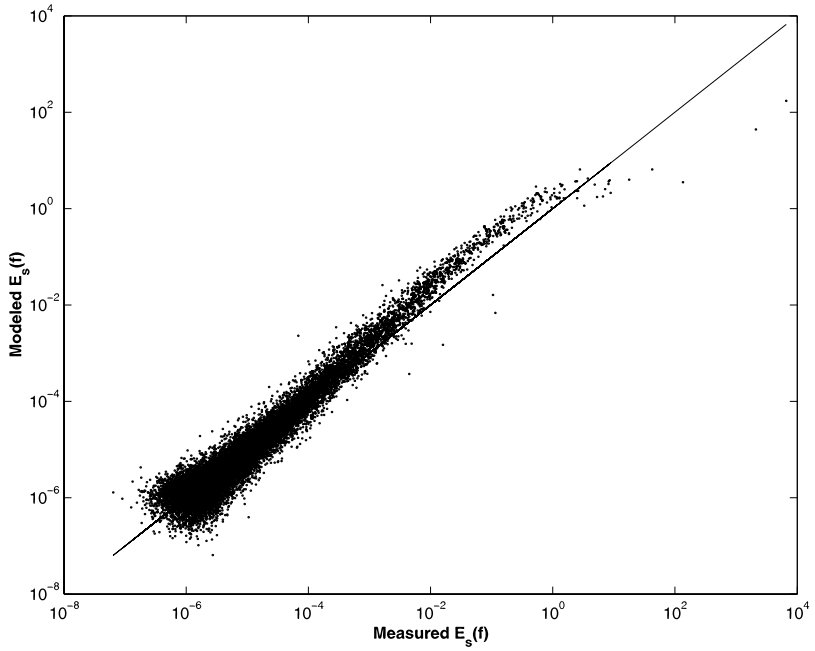

Figure 6. Comparison between measured and model 2 predictions of the soil moisture spectrum $E_s(f)$. The regression slope, intercept, and coefficient of determination r^2 are 0.93, −1.38, and 0.74, respectively. The 1:1 line is also shown for reference. Note the underestimation of the energetic components corresponding to the low frequencies.

of the memory timescale, we find that because $1/\beta_1$ (∼180 hours) occurs at frequencies much smaller than diurnal (∼12 hours), variability or energy in diurnal ET (evident in Figure 4) does not significantly impact $E_s(f)$. Hence, according to the analysis in Figure 7, it is safe to say that for modeling the spectrum of soil moisture, diurnal dynamics in ET may be ignored if $\beta_1^{-1} \gg 12$ hours, as is the case here. To further support this argument, we note that, in a separate study, it was shown that at the daily timescale the impact of rainfall variability on soil moisture dynamics is much stronger than fluctuations in evapotranspiration [*Daly and Porporato*, 2006].

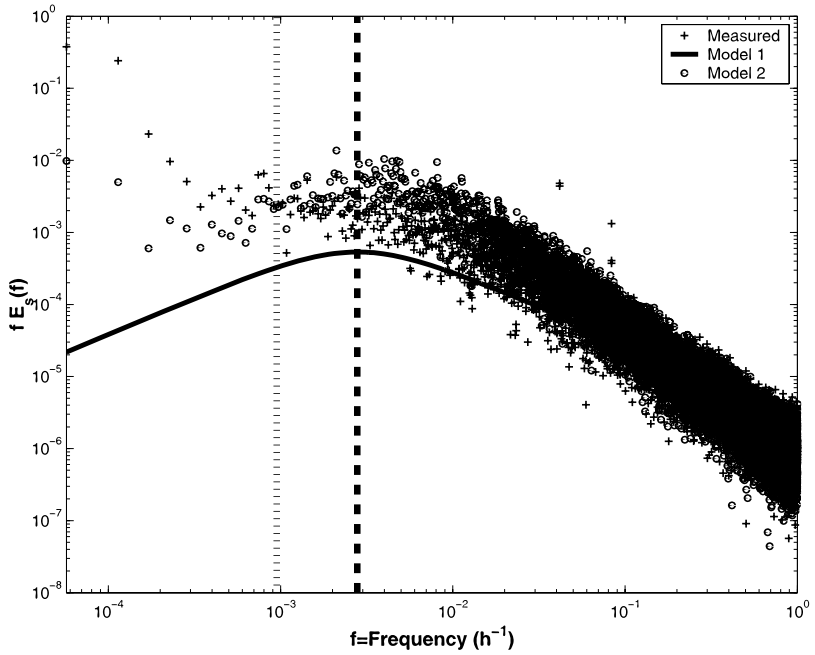

Figure 7. Comparison between measured and modeled $f E_s(f)$. Model 1 is the thick solid line, model 2 is in solid dots, and the measurements are pluses. The vertical lines are frequencies corresponding to the following timescales (right to left): ${\beta_1}^{-1}$ (= 7.6 days) determined from the peak of $f E_s(f)$ shown here and the measured integral timescale (= 42 days).

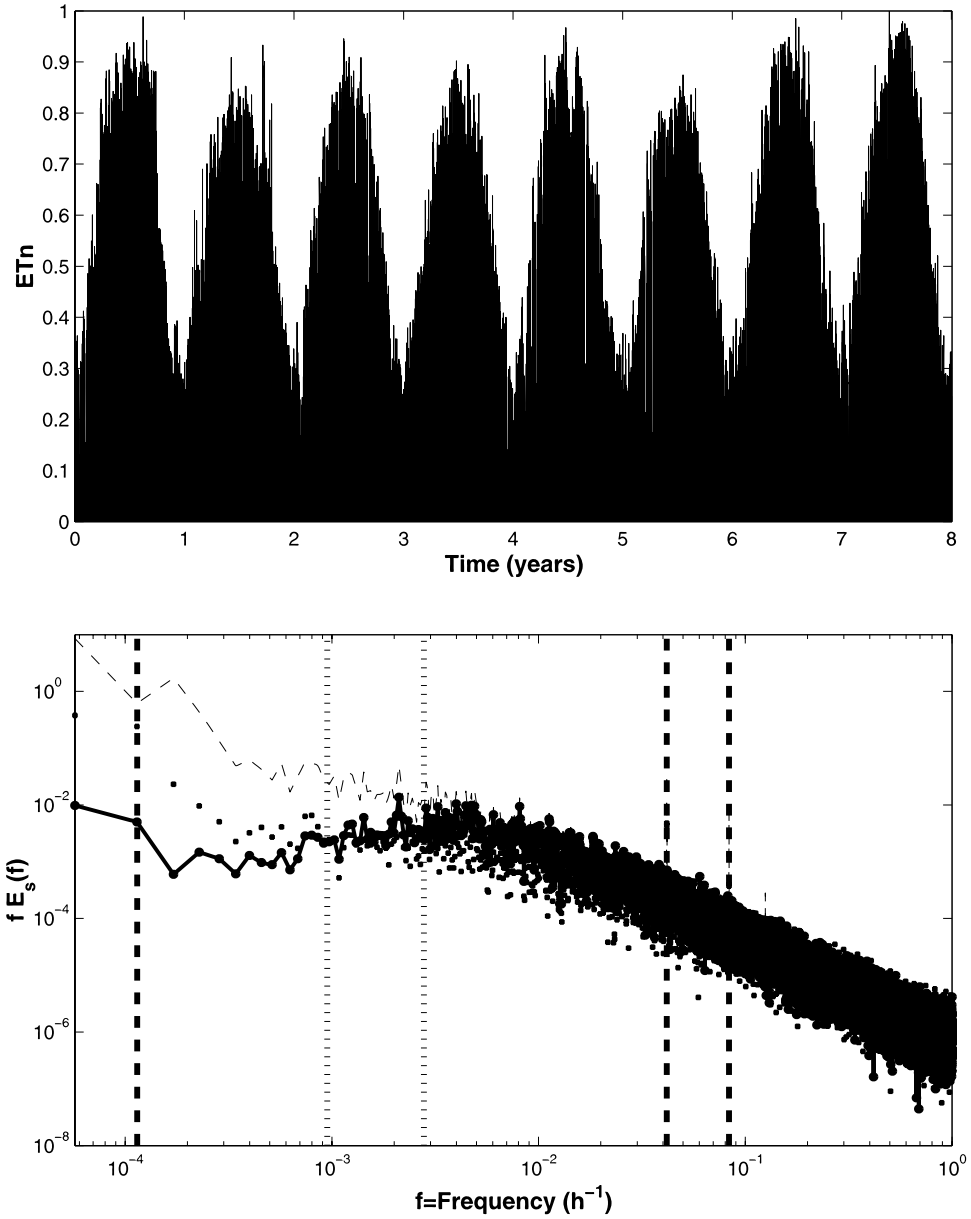

Figure 8. (top) Variations of normalized equilibrium evapotranspiration (ETn) with time (normalized by its maximum value). (bottom) Comparison between measured (symbols) and modeled (lines) $f E_s(f)$. Model 2 is the solid thick line, and model 3 is the dashed line. Note the large energy content at low frequencies for model 3.

[28] Both Figures 6 and 7 suggest that model 2 is missing some low-frequency energy not explained by precipitation, likely to be introduced by low-frequency variability in ET [*Stoy et al.*, 2006]. It is clear from Figure 4 that while the spectrum of precipitation appears almost white at frequencies lower than seasonal, the spectrum of soil moisture shares some attributes with the spectrum of ET for seasonal and longer timescales. A logical starting point to explore this hypothesis analytically is to assume that ET is not restricted by soil moisture content (which is unrealistic for all ranges of soil moisture) and is approximated by its equilibrium evaporation value (ET_{equ}), given by

$$\mathrm{ET}_{equ}(t) \approx c\frac{\Delta}{\Delta+\gamma}R_n(t) \tag{8}$$

where Δ and γ are the slope of the saturation vapor pressure − temperature curve and the psychometric constant, respectively, R_n is the net radiation measured above the canopy and c is necessary to convert W m^{-2} to mm h^{-1} (300 W m^{-2} are approximately 0.4 mm h^{-1}). As before, the Fourier coefficients of the soil moisture content at frequency f can be related to the Fourier coefficients of the precipitation and equilibrium evaporation via

$$S(f) = -\frac{P(f) - \mathrm{ET}_{equ}(f)}{if}. \tag{9}$$

[29] The resulting soil moisture spectrum is given by

$$E_s(f) = \frac{1}{f^2}\left|P(f) - \mathrm{ET}_{equ}(f)\right|^2 \tag{10}$$

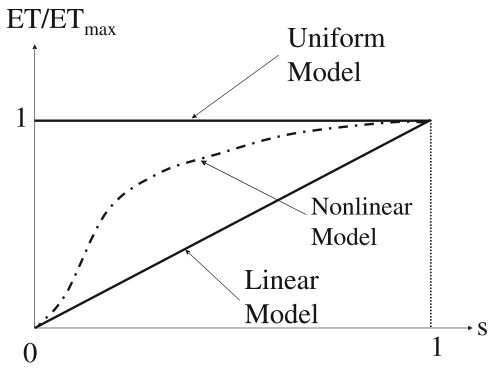

Figure 9. Variations of ET/ET$_{max}$ with s assuming linear (models 1 and 2) and constant or uniform dependence (model 3). Note that the combined linear and uniform models encompass all plausible nonlinear relationships between ET/ET$_{max}$ with s.

and is hereafter referred to as model 3. Notice that models 2 (linear dynamics) and 3 bound all plausible relationships between ET and s. As expected, the spectrum of model 3 is energetically unbounded (variance increases indefinitely) as the sampling time increases indefinitely ($f \to 0$), which is unrealistic and physically not plausible. Within the 8-year sampling period studied here, we expect that this spectrum overestimate the measured spectrum at low f. In fact, although for this spectrum the memory in soil moisture is not defined, yet the seasonal all the way up to interannual cycles in ET$_{equ}$ retain their fingerprints in the soil moisture (see Figure 8). What Figure 8 demonstrates then is that the measured soil moisture content spectrum is bounded between models 2 and 3 and that the missing "energy" at low frequencies (say $f \ll \beta_1$) in model 2 appears to be attributed to a partial "decoupling" between ET and s at seasonal timescales with ET now being driven primarily by available energy (or equilibrium evaporation conditions). Note that if we linearly combine the spectra (i.e., additive variance) in equations (7) and (10), we obtain

$$E_s(f) = a_1 \frac{|P(f)|^2}{\beta_1^2 + f^2} + (1 - a_1) \frac{|P(f) - \mathrm{ET}_{equ}(f)|^2}{f^2} \qquad (11)$$

where $a_1 \in [0, 1]$ now measures the degree of nonlinearity in the ET $-$ s relationship of Figure 9. Even if a_1 is close to unity (but not exactly unity), as $f \to 0$, the spectrum in equation (11) will be dominated by the second term, and

$$E_s(f) \to (1 - a_1) \frac{|P(f) - \mathrm{ET}_{equ}|^2}{f^2}.$$

further confirming this hypothesis for energy-limited ecosystems.

5. Summary and Conclusions

[30] We proposed a simplified analytical model for the spectrum of soil moisture content at scales ranging from hour to interannual timescales for a site whose hydrologic balance is primarily governed by stored water, rainfall, and ET. We showed that for this simplified hydrologic balance, when ET is linearly related to soil moisture content and when the precipitation spectrum is approximately white noise, the resulting spectrum becomes red (decaying at f^{-2}) at high frequencies and white at low frequencies. The soil moisture memory can be predicted analytically as $\frac{1}{\beta_1} = \frac{\eta R_L}{\mathrm{ET}_{max}}$. We also showed that the origin of the measured spectral decay in the soil moisture spectrum that is "steeper" than f^{-2} (about $f^{-2.75}$) could be explained by the decay in the measured precipitation spectrum (roughly as $f^{-0.75}$) for higher frequencies (i.e., $f \gg \beta_1$). This rapid spectral decay at high frequencies makes the soil moisture variance highly imbalanced in the frequency domain. To quantitatively illustrate this point using only the soil moisture time series measurement, we showed that 99.4% of the soil moisture variance could be described by using less than 0.4% Fourier modes. A practical outcome of this energy imbalance in the frequency domain is that the diurnal cycle in ET can be ignored if $\beta_1^{-1} \gg 12$ hours (at least for the analysis of θ variability). Both models, however, underestimated the measured soil moisture content energy spectrum at low frequencies ($f \ll \beta_1$). We argued that this underestimation could be traced back to a decoupling between ET and soil moisture at the seasonal timescale, presumably because of the strong coupling between ET and available energy. Considering only the primary external drivers of ET, R_n and vapor pressure deficit (D), 69% of the half hour variability in ET is explainable by R_n and 43% by D despite the low values of the decoupling coefficient (Ω, [*Jarvis and McNaughton*, 1986]) for this stand [*Stoy et al.*, 2006]. This result (that ET is primarily energy limited) also agrees with combined results from other pine plantations in the southeastern United States [*Gholz and Clark*, 2002] that showed strong relationships between annual and seasonal ET and R_n and suggest that improved understanding of θ dynamics in the frequency domain in "energy-limited" ecosystems may be obtained by focusing on this long-term forcing.

Appendix A: Inferring β_1 From the Spectrum of a Finite Time Series

[31] The memory of a zero-mean and unit variance stochastic process is often determined from the correlation time (or 1/e point, here β_1^{-1}) or the integral timescale (Γ). These quantities can be determined from the spectral density function $E(f)$ by noting that Γ, the autocorrelation function $\rho(\tau)$, and $E(f)$ are all related by

$$\Gamma = \int_0^\infty \rho(\tau) d\tau,$$

$$\rho(\tau) = \int_{-\infty}^{+\infty} e^{i\tau f} E(f)\, df, \qquad \text{and}$$

$$E(f) = \frac{1}{2\pi} \int_{-\infty}^{+\infty} e^{-if\tau} \rho(\tau) d\tau.$$

Hence Γ can be directly inferred from $E(f)$ when $f = 0$ because

$$E(0) = \frac{1}{2\pi} \int_{-\infty}^{+\infty} e^0 \, \rho(\tau) \, d\tau = \frac{1}{\pi} \int_{0}^{+\infty} \rho(\tau) \, d\tau = \frac{\Gamma}{\pi}.$$

For a time series sampled over a finite time interval, $E(0)$ is difficult to determine without (heuristic) extrapolations.

[32] In our case, the spectrum of the model (i.e., model 1) follows the canonical form

$$E(f) = \frac{\sigma^2}{\beta_1^2 + f^2},$$

where $\sigma^2 = \frac{\beta_1}{\pi}$ to ensure a unit variance for all $f \in [0, \infty]$. With this estimate of σ^2,

$$\Gamma = \frac{1}{\beta_1}.$$

[33] Furthermore, β_1 can be determined as the frequency at which $U(f) = f\,E(f)$ is maximized. This β_1 estimate, derived from the maximum of $U(f)$, can be demonstrated by noting that

$$\frac{dU(f)}{df} = -\frac{2\sigma^2 f^2}{\left(\beta_1^2 + f^2\right)^2} + \frac{\sigma^2}{\beta_1^2 + f^2} = 0 \text{ (i.e., maximum)}$$

only when $f = \pm\beta_1$ (and we only accept positive frequencies).

[34] In short, by plotting f (as abscissa) versus $f\,E(f)$ (as ordinate) and determining the frequency at which the ordinate peaks provides a clear estimate of β_1 (and Γ) without requiring an extrapolation for $E(0)$.

[35] **Acknowledgments.** This research was supported by the Office of Science (BER), U.S. Department of Energy, through its Southeast Regional Center (SERC) of the National Institute for Global Environmental Change (NIGEC) under cooperative agreement DE-FC03-90ER61010, through BER's FACE FACTS-I project, grant DE-FG02-95ER62083, through the Terrestrial Carbon Processes Program (TCP), and by the National Science Foundation (NSF-EAR-0208258).

References

Amenu, G. G., P. Kumar, and X. Z. Liang (2005), Interannual variability of deep-layer hydrologic memory and mechanisms of its influence on surface energy fluxes, *J. Clim.*, *18*, 5024–5045.

Chen, J., and P. Kumar (2002), Role of terrestrial hydrologic memory in modulating ENSO impacts in North America, *J. Clim.*, *15*, 3569–3585.

Daly, E., and A. Porporato (2006), Impact of hydroclimatic fluctuations on the soil water balance, *Water Resour. Res.*, *42*, W06401, doi:10.1029/2005WR004606.

Delworth, T., and S. Manabe (1988), The influence of potential evaporation on the variabilities of simulated soil wetness and climate, *J. Clim.*, *1*, 523–547.

Delworth, T., and S. Manabe (1993), Climate variability and land-surface processes, *Adv. Water Resour.*, *16*, 3–20.

D'Odorico, P., F. Laio, A. Porporato, and I. Rodriguez-Iturbe (2003), Hydrologic controls on soil carbon and nitrogen cycles. II. A case study, *Adv. Water Resour.*, *26*, 59–70.

Entekhabi, D., I. Rodriguez-Iturbe, and F. Castelli (1996), Mutual interaction of soil moisture state and atmospheric processes, *J. Hydrol.*, *184*, 3–17.

Findell, K. L., and E. A. B. Eltahir (1997), An analysis of the soil moisture-rainfall feedback based on direct observations from Illinois, *Water Resour. Res.*, *33*, 725–735.

Gholz, H. L., and K. L. Clark (2002), Energy exchange across a chronosequence of slash pine forests in Florida, *Agric. For. Meteorol.*, *112*, 87–102.

Jarvis, P. G., and K. G. McNaughton (1986), Stomatal control of transpiration—Scaling up from leaf to region, *Adv. Ecol. Res.*, *15*, 1–49.

Kaimal, J. C., and J. Finnigan (1994), *Atmospheric Boundary Layer Flows: Their Structure and Measurement*, 289 pp., Oxford Univ. Press, New York.

Katul, G., and B. Vidakovic (1996), The partitioning of attached and detached eddy motion in the atmospheric surface layer using Lorentz wavelet filtering, *Boundary Layer Meteorol.*, *77*, 153–172.

Katul, G., and B. Vidakovic (1998), Identification of low-dimensional energy containing flux transporting eddy motion in the atmospheric surface layer using wavelet thresholding methods, *J. Atmos. Sci.*, *55*, 377–389.

Katul, G., R. Oren, D. Ellsworth, C. I. Hsieh, N. Phillips, and K. Lewin (1997), A Lagrangian dispersion model for predicting CO_2 sources, sinks, and fluxes in a uniform loblolly pine (*Pinus taeda* L) stand, *J. Geophys. Res..*, *102*, 9309–9321.

Katul, G. G., C. D. Geron, C. I. Hsieh, B. Vidakovic, and A. B. Guenther (1998), Active turbulence and scalar transport near the forest-atmosphere interface, *J. Appl. Meteorol.*, *37*, 1533–1546.

Koster, R. D., and M. J. Suarez (2001), Soil moisture memory in climate models, *J. Hydrometeorol.*, *2*, 558–570.

Koster, R. D., et al. (2004), Regions of strong coupling between soil moisture and precipitation, *Science*, *305*, 1138–1140.

Lauzon, N., F. Anctil, and J. Petrinovic (2004), Characterization of soil moisture conditions at temporal scales from a few days to annual, *Hydrol. Processes*, *18*(17), 3235–3254.

Oren, R., B. E. Ewers, P. Todd, N. Phillips, and G. Katul (1998), Water balance delineates the soil layer in which moisture affects canopy conductance, *Ecol. Appl.*, *8*, 990–1002.

Parlange, M. B., G. G. Katul, R. H. Cuenca, M. L. Kavvas, D. R. Nielsen, and M. Mata (1992), Physical basis for a time series model of soil water content, *Water Resour. Res.*, *28*, 2437–2446.

Porporato, A., E. Daly, and I. Rodriguez-Iturbe (2004), Soil water balance and ecosystem response to climate change, *Am. Nat.*, *164*, 625–632.

Priestley, M. B. (1981), *Spectral Analysis and Time Series*, 877 pp., Elsevier, New York.

Schäfer, K. V. R., R. Oren, C. T. Lai, and G. G. Katul (2002), Hydrologic balance in an intact temperate forest ecosystem under ambient and elevated atmospheric CO_2 concentration, *Global Change Biol.*, *8*, 895–911.

Stoy, P., G. G. Katul, M. Siqueira, J. Y. Juang, H. R. McCarthy, H. S. Kim, C. Oishi, and R. Oren (2005), Variability in net ecosystem exchange from hourly to inter-annual time scales at adjacent pine and hardwood forests: A wavelet analysis, *Tree Physiol.*, *25*, 887–902.

Stoy, P. C., G. G. Katul, M. B. S. Siqueira, J.-Y. Juang, H. R. McCarthy, A. C. Oishi, J. M. Uebelherr, H.-S. Kim, and R. Oren (2006), Separating the effects of climate and vegetation on evapotranspiration along a successional chronosequence in the southeastern U.S., *Global Change Biol.*, *12*, 1–21.

Webb, E. K., G. I. Pearman, and R. Leuning (1980), Correction of flux measurements for density effects due to heat and water-vapor transfer, *Q. J. R. Meteorol. Soc.*, *106*, 85–100.

Wilson, K. B., P. J. Hanson, P. J. Mulholland, D. D. Baldocchi, and S. D. Wullschleger (2001), A comparison of methods for determining forest evapotranspiration and its components: Sap-flow, soil water budget, eddy covariance and catchment water balance, *Agric. For. Meteorol.*, *106*, 153–168.

Wu, W. R., and R. E. Dickinson (2004), Time scales of layered soil moisture memory in the context of land-atmosphere interaction, *J. Clim.*, *17*(14), 2752–2764.

Wu, W. R., M. A. Geller, and R. E. Dickinson (2002), The response of soil moisture to long-term variability of precipitation, *J. Hydrometeorol.*, *3*(5), 604–613.

E. Daly, J.-Y. Juang, G. G. Katul, H.-S. Kim, A. C. Oishi, A. Porporato, M. B. Siqueira, and P. C. Stoy, Nicholas School of the Environment and Earth Sciences, Box 90328, Duke University, Durham, NC 27708-0328, USA. (gaby@duke.edu)